Advent of a Wide-Band-Gap Semiconducting Low-Density Material Possessing Significantly High Specific Hardness

Arvind Kumar Jaiswal, Barnali Maji, Jitamanyu Chakrabarty, Chandan Mondal, and Joydeep Maity

(Submitted April 12, 2020; in revised form May 25, 2020; published online July 3, 2020)

The tetragonal crystalline form of boron nitride remains in theoretical prediction stage till date without being synthesized in real practice and in accordance; properties could not be verified experimentally. Here we synthesize tetragonal boron nitride through a low-cost chemical synthesis route for the first time along with thermodynamic analysis and identification of evolved product gases through gas chromatography to authenticate the chemical reaction feasibility. The evolution of tetragonal boron nitride is substantiated with XRD analysis, Raman spectroscopy, x-ray photoelectron spectroscopy and FEG-TEM based SADP and EDS analysis together with IFFT micrograph-based measurement of the interplanar spacing of dominating (110) growth plane. The experimentally measured lattice parameters (a = 0.4378 nm, c = 0.2541 nm) closely match with those predicted theoretically (a = 0.4380 nm, c = 0.2540 nm). The presence of sp^3 bonding in synthesized material is also confirmed by Raman spectroscopy and x-ray photoelectron spectroscopy. Furthermore, we determine some significant properties of synthesized tetragonal boron nitride that envisage large optical band gap (5.66 eV), low electrical conductivity (671 S m^{-1}) of semiconducting range, low density (1.83 g cm^{-3}), high hardness (28 GPa) and the highest specific hardness (15.30 GPa/g cm^{-3}) among other forms of polycrystalline boron nitride and commonly used hard ceramic materials. Accordingly, a new dimension is hereby added to material development for electronic/optoelectronic applications as well as in low-density hard structural material synthesis in view of using tetragonal boron nitride as reinforcement for metal matrix composites.

1. Introduction

Different polymorphs of boron nitride (BN) have gained tremendous significance in material science and technology with regard to their unique properties. Cubic BN, in polycrystalline form, possesses very high hardness ranging from 33 to 45 GPa (Ref 1-3). As a special case, in nanotwinned form, it also exhibits exceptionally high hardness [95-108 GPa (Ref 1)]. Furthermore, low electrical conductivity (10^{-8} S m^{-1}) and large optical band gap (6.1-6.4 eV) are the other significant characteristics of cubic BN (Ref 4). On the other hand, the wurtzite form of BN is also very hard [hardness = 46 GPa (Ref 5)] along with a large optical band gap [4.5-5.5 eV (Ref 4)]. Hexagonal BN, though relatively much softer [hardness = 0.08 GPa (Ref 6)], exhibits large band gap [5.96 eV (Ref 7)] and low electrical conductivity [10^{-11}-10^{-13} S m^{-1} (Ref 8)]. Besides, the density of BN is relatively higher in cubic [3.45 g cm^{-3} (Ref 4)] and wurtzite form [3.49 g cm^{-3} (Ref 9)] than in hexagonal form [2.275 g cm^{-3} (Ref 8)]. These three polymorphs (cubic, hexagonal and wurtzite) of BN have been synthesized in real practice along with their property characterization. Beyond these approaches, in recent years, a novel polymorph of BN possessing a body-centered tetragonal crystal structure has been theoretically predicted (Ref 10-13). Although cubic and hexagonal forms of BN are known to exhibit insulating behavior, a semiconducting nature is theoretically predicted for tetragonal BN by Wen et al. (Ref 10). Furthermore, as per theoretical conceptualization, being built up by sp^3 bonds, tetragonal BN is expected to possess mechanical properties comparable to cubic BN (Ref 10). Furthermore, the theoretically predicted average hardness of this novel tetragonal polymorph approaches that of cubic BN, thereby indicating a possible advent of new hard material (Ref 11). Besides, ab initio calculations also indicate a low density and large band gap of tetragonal BN (Ref 12) so as to exemplify feasibility of further potential application (Ref 13). However, tetragonal BN still exists in the domain of theoretical speculations and yet to be synthesized in real practice. In the present research work, we successfully synthesize tetragonal BN through a low-cost chemical route. We further determine its significant properties (band gap, electrical conductivity, density and hardness) through experimentation in view of potential futuristic applications.

Arvind Kumar Jaiswal, Barnali Maji, and **Joydeep Maity**, Department of Metallurgical and Materials Engineering, National Institute of Technology Durgapur, Durgapur, West Bengal 713209, India; **Jitamanyu Chakrabarty**, Department of Chemistry, National Institute of Technology Durgapur, Durgapur, West Bengal 713209, India; and **Chandan Mondal**, Rolling and Formability Group, Defence Metallurgical Research Laboratory, Kanchanbagh, Hyderabad 500058, India. Contact e-mails: joydeep_maity@yahoo.co.in and joydeep.maity@mme.nitdgp.ac.in.

2. Experimental Procedure

In the present investigation, synthesis of BN was carried out using a low-cost chemical reaction route by stirring (at 600 rpm) an aqueous solution containing 8.27 g boric acid and 4 g urea (taken in 2:1 molar ratio) dissolved in 100 ml distilled water for 2 h at 80 °C. The precipitated particles were thereafter filtered and dried in an oven at 150 °C for 30 min. The synthesized BN particles were at first studied in a field emission scanning electron microscope (FESEM, Model: SIGMA, Zeiss, Germany), primarily to reveal morphology and particle size. The size of synthesized particle was measured from FESEM images as the diameter of a circle possessing an area equal to the area covered by the particle in two-dimensional image. X-ray diffraction (XRD) analysis of synthesized particle was carried out at slow scan rate in a high-resolution x-ray diffractometer (X'Pert PRO, PANalytical B.V., PW3040/60, The Netherlands) using Cu K$_\alpha$ radiation ($\lambda = 0.15406$ nm). The overall phase analysis was carried out in a wide scan range ($2\theta = 20°$-$90°$) at a scan rate of $0.5°$ min^{-1}. Besides, the main dominant peak was contemplated upon at a selected scan range around it ($2\theta = 25°$-$29°$) under an extremely slow scan rate of $0.25°$ min^{-1}. Subsequently, Raman spectroscopy of the synthesized particle was carried out in a Raman spectrometer (alpha300, WITEC, Germany) using a wavelength of 530 nm. X-ray photoelectron spectroscopy (XPS) analysis was also carried out using an Omicron Nanotechnology Spectrometer (model: ESCA + , UK) equipped with the high transmission Argus CU hemispherical analyzer and high-power monochromatic Al K$_\alpha$ x-ray source. The aforementioned features were specifically synchronized to obtain the highest sensitivity for quantitative XPS analysis.

The synthesized particles were further characterized in a high-resolution transmission electron microscope equipped with field emission gun (FEG-TEM, Model: JEM-2100F, JEOL, Japan) in terms of morphological appearance, selected area electron diffraction pattern (SADP), energy-dispersive x-ray spectroscopy and lattice image with inverse fast Fourier Transform (IFFT) treatment. Furthermore, during synthesis of BN, evolution of gaseous phases was realized. In order to analyze the evolved gas mixture, the chemical synthesis was carried out in a typical Schlenk flask. The Schlenk flask was evacuated at the beginning to avoid any environmental contamination. Thereafter, the evolved gases were collected in another vacuum Schlenk flask. Prior to the analysis of gas mixture by gas chromatography (GC); the flask containing gas mixture was exposed to sub-zero temperature (-20 °C) in a freezer so as to separate out any suspected water vapor through condensation, thereby avoiding any damage of GC column. The exposure to sub-zero temperature eventually resulted in condensation of water vapor on the inner wall of the flask indicating evolution of water vapor during chemical reaction. Subsequently, the remaining gas mixture was subjected to analysis in a gas chromatograph (Model No. QP 2020, Shimadzu, Japan) using thermal conductivity detector. Optical band gap of synthesized particles was determined by ultraviolet–visible (UV–Vis) spectroscopy in a UV–Vis spectrometer (model No. UV-1800, Shimadzu, Japan). Photons with wavelengths in a range of 200-1100 nm were passed through the BN particles suspended in ethanol, and absorbance was recorded. Synthesized BN particles were sealed inside a copper tube (5 mm in inner diameter and 14 mm in height) and subse-

quently sintered with 2 h of holding at 800 °C under 0.12 MPa pressure. The electrical conductivity of this sintered BN specimen was evaluated by a four-probe method (4-probe Keithley 6221 Nanovoltmeter, Japan), using a constant input current of 0.1 A with a probe length of 10 mm. Density being an important property in the present investigation, a detailed density measurement techniques were adopted for as-synthesized BN particles and sintered BN pellet. At first, density of synthesized BN particles (obtained in powder form) was measured with normal water displacement method (using graduated measuring cylinder containing water and analytical balance) with respect to rise in the level of water in cylinder on incorporation of particle and corresponding change in mass. Again, the density of synthesized powdery BN particles was measured in a gas pycnometer (Ultrapyc 1200e, Quantachrome Instruments, USA) for cross-verification of results. In case of sintered BN pellet, at first the density was determined with direct approach of weighing the pellet of known dimension (therefore the known volume). Thereafter, for cross-verification, the density of sintered BN pellet was again determined using a high precision density measurement kit (CPA225D, Sartorius, Germany) with respect to measured mass in air and in water. Finally, hardness of the sintered BN specimen was measured in a Vickers microhardness testing machine (MMT-X7B, Hibiki Co., Japan) at 25 gf load.

3. Results and Discussion

3.1 Morphological Appearance in FESEM Study

The synthesized particles are shown in FESEM micrographs (Fig. 1a and b). The size range of these synthesized particles, as measured from low-magnification FESEM micrograph (Fig. 1a), is 1-12 μm with a mean size of 7 ± 3 μm. The high-magnification FESEM micrograph of a single particle exhibits a glittering crystalline appearance (Fig. 1b). Furthermore, the synthesized particle exhibits a typical 'faceted surface,' which indicates toward growth of a preferred plane during crystallization.

3.2 Ascertaining Crystal Structure by XRD

The results of x-ray diffraction (XRD) analysis are shown in Fig. 2(a) and (b) for overall scan ($2\theta = 20°$-$90°$) and selected short-range scan ($2\theta = 25°$-$29°$), respectively. It is interesting to note that the intensity of one peak is significantly higher than other peaks. Such a typical XRD pattern is obtained on repeated occasions, thereby exemplifying its authenticity. According to the latest standard literature (Ref 14, 15), such a typical x-ray diffractogram is obtained owing to preferred growth of a particular plane during crystallization. This is also supported by the observed 'faceted surface' of synthesized BN particle in the present investigation (Fig. 1b). Furthermore, the selected short-range scan around this strongest peak accurately predicts corresponding diffraction angle (2θ) as $28.25°$ (Fig. 2b). Among all polymorphs of boron nitride (BN), it is nearest to BN possessing tetragonal crystal structure which appears at $28.803°$ for (110) diffraction plane as per standard diffraction data file (Ref 16). This should not be confused with (002) diffraction peak of hexagonal BN (Ref 17) likely to appear at $26.746°$, since no peak is found in a range: $26°$-$27°$ (Fig. 2b). Similar to the present investigation, such a preferred growth of
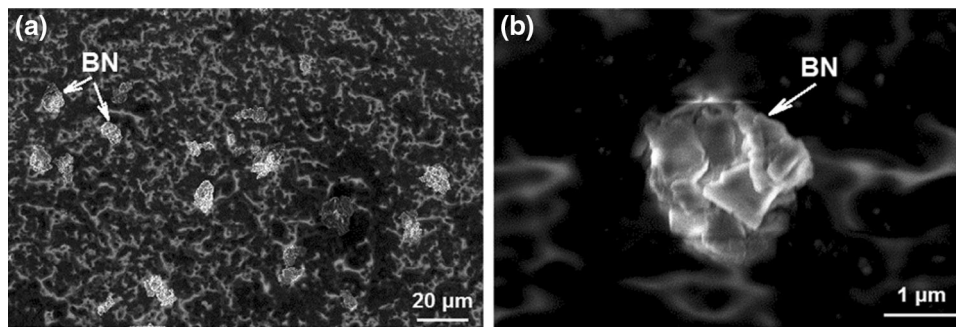
Fig. 1 FESEM micrographs of synthesized BN particles: (a) many particles (at low magnification); (b) single particle (at high magnification)

(110) plane has been reported for many other tetragonal crystals, namely $MnSn_2$ (Ref 18), TiO_2 (Ref 19), SnO_2 (Ref 20) and NbO_2 (Ref 21). The fundamental analysis on atomic packing in body-centered tetragonal structure by Dunlop (Ref 22) identifies (110) plane to possess closer atomic packing as compared to other planes. Furthermore, as per basic conceptualization, close packing of atoms pertains to a lower energy (Ref 23-25). Therefore, in the present investigation, body-centered tetragonal crystal structure of BN is stabilized through preferred growth of (110) plane possessing close atomic packing, thereby reducing the system energy. This is reflected as the strongest (110) diffraction peak in XRD analysis (Fig. 2a). Besides, only one more peak pertaining to diffraction from (011) plane of tetragonal BN is practically identifiable at $2\theta = 40.87°$, though of small intensity (8% of the (110) peak intensity). As per standard diffraction data file (Ref 16), (011) diffraction for tetragonal BN must ideally occur at $2\theta = 41.045°$. Therefore, with regard to diffraction data file (Ref 17), the position of (010) diffraction peak for hexagonal BN (at $2\theta = 41.614°$) is relatively more away from the obtained peak position (at $2\theta = 40.87°$) as compared to (011) diffraction peak for tetragonal BN ($2\theta = 41.045°$). In accordance, the crystal structure of synthesized BN is hereby preliminarily identified as 'tetragonal' and not as 'hexagonal.' All other small peaks in Fig. 2(a) possess an intensity less than 5% of the intensity of (110) diffraction peak. Therefore, these cannot be distinguished from background radiation arising due to incoherent scattering and accordingly are not indexed. Even then within this domain, the small peak at $2\theta = 46°$ (about 4% of the intensity of (110) peak) would be identified as (111) diffraction peak of tetragonal BN as per the standard literature (Ref 16). Furthermore, with regard to the prominent (110) diffraction peak, the crystallite size (D) of synthesized BN may be calculated using well-known Scherrer formula: $D = \frac{0.94 \times \lambda}{\beta \mathrm{Cos}\theta}$. Considering (110) peak (main diffraction peak), the measured values of 2θ and β (full width at half maxima) are $28.25°$ and $0.05°$ (8.7266×10^{-4} rad), respectively (Fig. 2b). Accordingly, for a wavelength (λ) of 0.15406 nm corresponding to Cu K_α radiation, the crystallite size of synthesized BN is found to be 171 nm.

3.3 Understanding the Nature of Bonding by Raman Spectroscopy

The evolution of BN is further introspected with Raman spectroscopy in view of phonon split-up phenomenon, as indicated in the standard literature (Ref 26). In case of Raman spectroscopy of cubic BN that possesses a sp^3-bonded three-dimensional structure, the triply degenerate phonon splits into transverse optical (TO) and longitudinal optical (LO) components within a range of 1000-1310 cm^{-1} (Ref 27-29). However, for hexagonal BN possessing a sp^2-bonded structure, the Raman active high energy phonon has a doubly degenerate in-plane optical mode at 1364 cm^{-1}, which does not exhibit an LO-TO splitting (Ref 30, 31). The result of Raman spectroscopy analysis of synthesized BN is shown in Fig. 2(c), where the characteristic LO-TO splitting is observed within the stipulated range (1000-1310 cm^{-1}). This confirms the existence of sp^3-type bonding in synthesized BN. The absence of any peak around 1364 cm^{-1} eliminates the possibility of the presence of sp^2-bonded hexagonal BN.

3.4 Ascertaining Bonding Characteristics by XPS

The final verification of the sp^3-bonded structure in synthesized BN is established with x-ray photoelectron spectroscopy (XPS) at core level excitation with monochromatized Al K_α radiation. The key results of this investigation are summarized in Fig. 2(d), (e), and (f). A long-range survey scan for B-1s core level (Fig. 2d) does not exhibit any π-plasmon peak around 200 eV binding energy level. According to the standard literature (Ref 32-34), the absence of π-plasmon peak around 200 eV binding energy level eliminates any possibility of the presence of sp^2-bonded hexagonal BN as the bulk phase. Furthermore, a high-resolution scan is carried out to ascertain 1 s core level peaks for B and N. The resultant XPS spectra for high-resolution scan are shown in Fig. 2(e) and (f), where a single-line fit is found to be adequate to authenticate experimental data points. Accordingly, in the present investigation, the peaks pertaining to B-1s and N-1s levels appear at binding energy values of 192.45 eV and 400.7 eV, respectively (Fig. 2e and f). With regard to the standard literature (Ref 35), in case of sp^2-bonded hexagonal BN, corresponding binding energy values are 190.4 eV and 398.12 eV for B-1s and N-1s levels, respectively. Therefore, in the present investigation, these binding energy values are shifted toward higher energy values with respect to sp^2-bonded hexagonal BN. In view of existing conceptualization (Ref 32, 35), this indicates the presence of sp^3-bonded structure of higher binding energy, as also substantiated in the present investigation with Raman spectroscopy by phonon split-up phenomenon (Fig. 2c).

3.5 Interpretation of Crystal Structure from FEG-TEM Results

While sp^3 bonding is confirmed by Raman spectroscopy and x-ray photoelectron spectroscopy along with initial verification
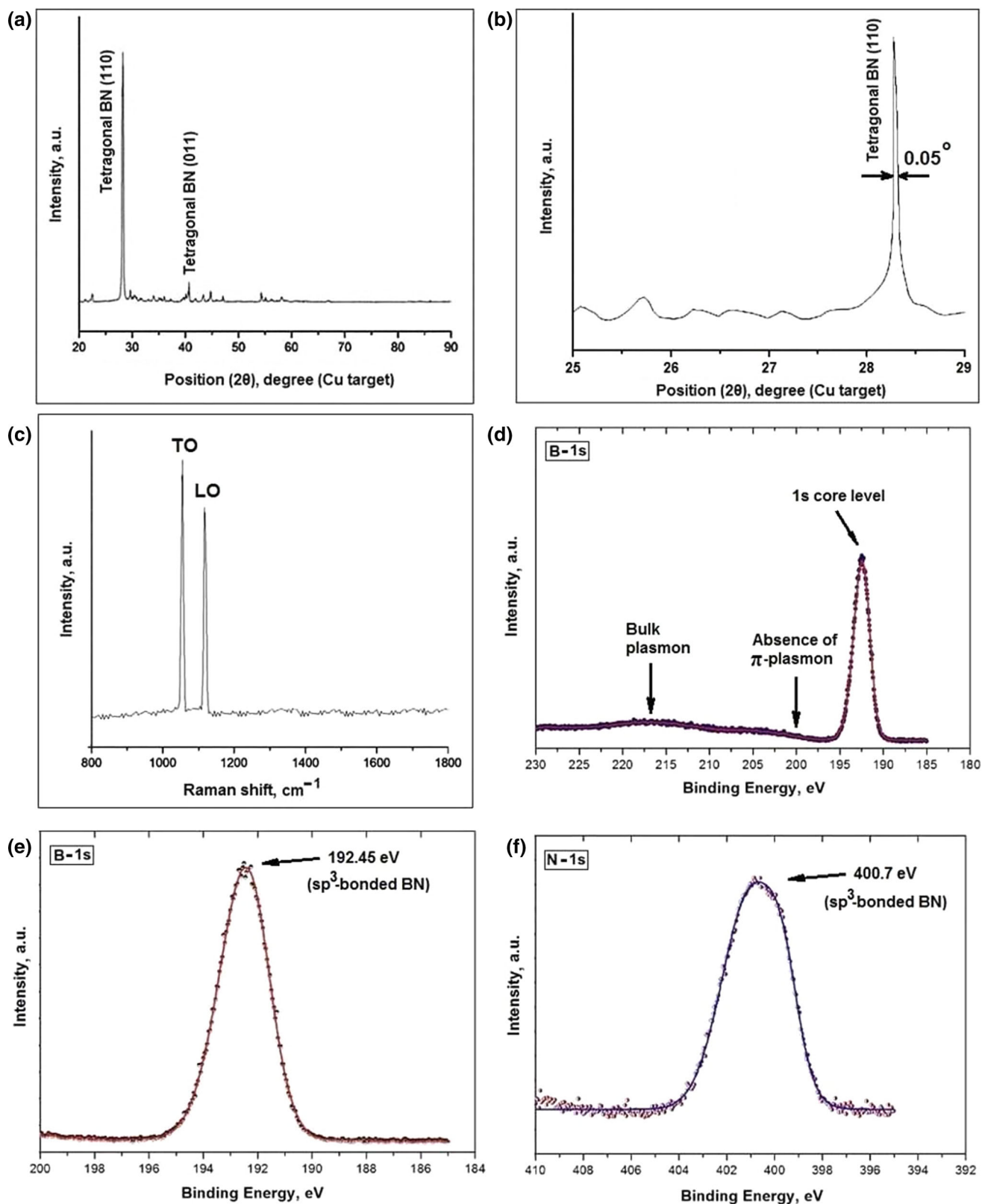
Fig. 2 Characterization of synthesized BN particles: x-ray diffractogram for (a) long-range scan and (b) short-range scan; (c) Raman spectra; XPS spectra obtained with (d) long-range survey scan for B-1s core level, (e) high-resolution scan around B-1s core level and (f) high-resolution scan around N-1s core level

of body-centered tetragonal crystal structure through XRD analysis, further confirmation of this newly synthesized material is of utmost necessity in view of lattice parameters of the concerned space lattice as exemplified in FEG-TEM study. The FEG-TEM bright field micrograph (Fig. 3a) shows a single BN particle consisting of several small crystals (crystallites) of BN with a measured mean size of 163 ± 32 nm. This measured crystallite size closely matches with that (171 nm) obtained from XRD results using Scherrer formula. Accordingly, the representative selected area electron diffraction pattern (SADP) exhibits spotted rings (Fig. 3b). Such a typical SADP is obtained on repeated occasions to authenticate its validity. When indexed SADP, a tetragonal BN structure is again identified, and in concurrence with XRD analysis (Fig. 2a), the ring pertaining to (110) diffracting plane appears to be the most prominent one consisting of many spots (Fig. 3b). The other identifiable ring belongs to (011) diffraction (in concurrence

with XRD pattern), though consisting of only a few spots. The identified rings are marked accordingly with yellow-colored circles (Fig. 3b). The prominence of (110) diffraction plane again indicates preferred growth of this plane during the process of BN synthesis. Now, the well-known relationship between interplanar spacing (d_{hkl}) and lattice parameters (a, c) for a tetragonal lattice is given as: $\frac{1}{d_{hkl}^2} = \frac{h^2 + k^2}{a^2} + \frac{l^2}{c^2}$. Considering experimentally obtained SADP (Fig. 3b) in reciprocal lattice space, we get: $\frac{1}{d_{110}} = 3.23$ nm^{-1}, $\frac{1}{d_{011}} = 4.55$ nm^{-1}. Putting these values in the above relationship, lattice parameters are calculated as: $a = 0.4378$ nm, $c = 0.2541$ nm. These values closely match the predicted lattice parameters ($a = 0.4380$ nm, $c = 0.2540$ nm) of tetragonal BN as per standard diffraction data file (Ref 16). Besides, the evolution of BN is also identified with the presence of B and N in FEG-TEM-based EDS spectra obtained by spot analysis (Fig. 3c). Furthermore, FEG-TEM-based IFFT lattice image (Fig. 3d)
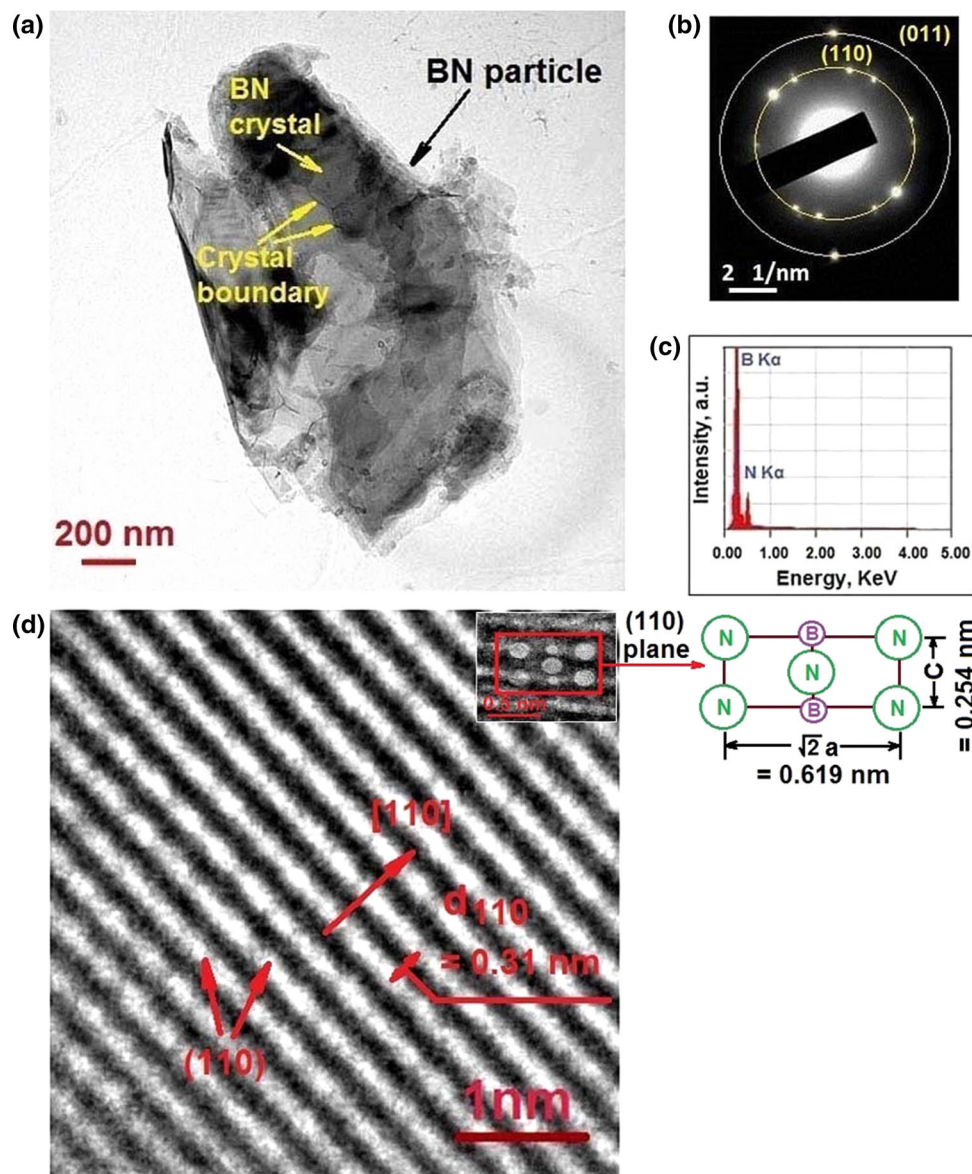
Fig. 3 FEG-TEM characterization of synthesized BN particle: (a) bright field image of a single particle consisting of many crystals; and its (b) SADP; (c) EDS spectra; (d) IFFT lattice image showing (110) planes (dominating growth planes) and inset exhibiting atomic arrangement on (110) plane
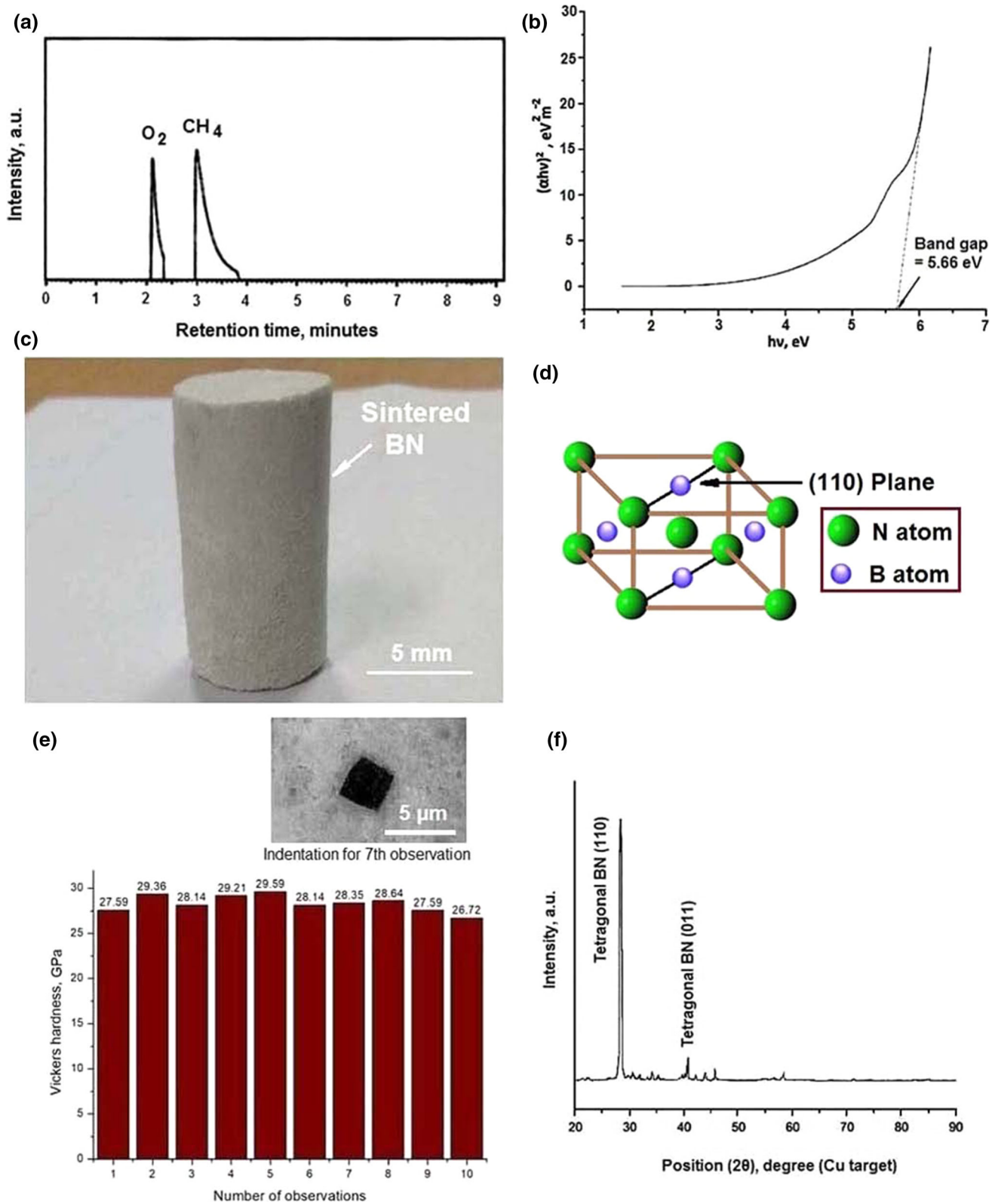
Fig. 4 (a) Results of gas chromatography test; (b) optical band-gap determination; (c) sintered BN specimen; (d) unit cell of the proposed body-centered tetragonal crystal structure of BN; (e) details of hardness test; (f) x-ray diffractogram of sintered BN specimen

Table 1 Properties of synthesized tetragonal BN

Material	Optical band gap, eV	Electrical conductivity, S m^{-1}	Density, g cm^{-3} (as-synthesized BN)	Density, g cm^{-3} (sintered BN)	Hardness, GPa
Synthesized tetragonal BN	5.66	671 ± 18	1.83 ± 0.02 (by water displacement method) 1.82 ± 0.02 (by Gas Pycnometer)	1.76 ± 0.01 (by high precision density measurement kit) 1.75 ± 0.02 (by direct approach)	28 ± 1

further exhibits (110) planes perpendicular to [110] direction. The measured interplanar spacing of (110) planes ($d_{110} = 0.31$ nm) closely matches with that (0.309713 nm) reported for tetragonal BN (Ref 16).

Therefore, with regard to foregoing characterization of synthesized BN particles, the evolution of sp^3-bonded tetragonal BN is confirmed in every respect (the crystal structure, lattice parameters and bonding characteristics) for the typical chemical synthesis route adopted in the present investigation. Furthermore, it is important to note that, so far in all previous prime research investigations accounting for chemical synthesis route (Ref 36, 37), at first boric acid and urea were mixed in desired proportion at room temperature in water/ethanol followed by drying to get solid mixture and subsequent firing at high temperature (600-950 °C) in N$_2$/NH$_3$ atmosphere so as to obtain hexagonal BN of low hardness, but possessing other unique properties. However, no one thought to activate the aqueous solution of boric acid and urea through stirring at a little elevated temperature (80 °C) so as to overcome the kinetic barrier for the synthesis of BN of tetragonal crystal structure through preferred growth of certain crystallographic plane, as achieved in the present investigation. Of course, optimizing reaction temperature and time needed several trials for many days in view of assuring almost complete conversion of reactants into desired product (tetragonal BN).

3.6 Chemical Reaction and Thermodynamic Analysis

Out of the evolved product gases, the evolution of methane (CH$_4$) and oxygen (O$_2$) is confirmed through gas chromatography analysis (Fig. 4a). Besides, as discussed earlier, evolution of water vapor (H$_2$O$_{(g)}$) as another gaseous product phase is confirmed through condensation of water vapor at sub-zero temperature inside the vacuum Schleck flask containing the product gas mixture. In view of the synthesis route adopted and identification of product gases, the following reaction scheme may be proposed for generation of BN:

$$2H_3BO_{3(aq)} + CO(NH_2)_{2(aq)} \rightarrow 2BN_{(s)} + CH_{4(g)} + 3H_2O_{(g)} + 2O_{2(g)}$$

$$(Eq\ 1)$$
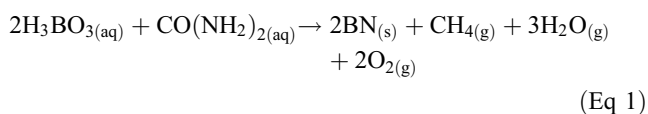
The standard Gibb's free energy change for this reaction is given as:

$$\Delta G^\circ = -RT \ln K \qquad (Eq\ 2)$$

The equilibrium constant (K) is expressed as:

$$K = \frac{a_{BN}^2 \times a_{CH_4} \times a_{H_2O}^3 \times a_{O_2}^2}{a_{H_3BO_3}^2 \times a_{CO(NH_2)_2}} \qquad (Eq\ 3)$$

where a_i stands for activity of species 'i' taking part in reaction as per Eq 1. Now, a_{BN} may be considered as 1 for solid state pure matter. Activities of the gaseous species may be replaced by their partial pressures (P_i). The activities of the species present in aqueous solution may be replaced by their mole fractions (X_i). Therefore, Eq 3 turns out to be:

$$K = \frac{P_{CH_4} \times P_{H_2O}^3 \times P_{O_2}^2}{X_{H_3BO_3}^2 \times X_{CO(NH_2)_2}} \qquad (Eq\ 4)$$

Considering partial pressure to be proportional to the mole fraction a gaseous species and the total number of moles of all gaseous species as per Eq 1 being 6, the values of P_{CH_4}, P_{H_2O} and P_{O_2} come out to be $\frac{1}{6}$, $\frac{3}{6}$ (i.e., $\frac{1}{2}$) and $\frac{2}{6}$ (i.e., $\frac{1}{3}$), respectively.

Initially, in order to synthesize BN, aqueous solution containing 8.27 g of boric acid (H$_3$BO$_3$) and 4 g of urea (CO(NH$_2$)$_2$) in 100 ml (100 g in mass) distilled water was taken. With regard to atomic mass values of H, B, O, C and N [1.008, 10.81, 16.00, 12.01 and 14.01 a.m.u., respectively (Ref 38)], the calculated values of the mass of one mole of H$_3$BO$_3$, CO(NH$_2$)$_2$ and solvent water are 61.834, 60.062 and 18.016 g, respectively. This accounts for 0.134, 0.067 and 5.551 mol of H$_3$BO$_3$, CO(NH$_2$)$_2$ and solvent water, respectively, in a total moles of 5.752 of initially taken solution. Therefore, mole fraction values of H$_3$BO$_3$ (i.e., $X_{H_3BO_3}$) and CO(NH$_2$)$_2$ (i.e., $X_{CO(NH_2)_2}$) are 0.023 and 0.012, respectively.

Accordingly, as per Eq 4: $K = \left[\frac{\frac{1}{6} \times \left(\frac{1}{2}\right)^3 \times \left(\frac{1}{3}\right)^2}{(0.023)^2 \times 0.012} \right] = 364.65$

Furthermore, considering the values of universal gas constant ($R = 8.314$ J mol^{-1} K^{-1}) and absolute reaction temperature ($T = 353$ K), as per Eq 2, ΔG° is obtained as $-17,312$ J mol^{-1}. Such a high negative value of ΔG° justifies the occurrence of the reaction represented in Eq 1. Further justification of the evolution of BN through reaction given by Eq 1 may be provided in terms of %conversion of initially taken solid reactants into the final solid product (BN). In reality, initially a total mass of 12.27 g solid reactants (8.27 g of H$_3$BO$_3$ and 4 g of CO(NH$_2$)$_2$) is taken. The mass of solid reaction product (BN) (after filtration of precipitated particle and oven drying to remove any adsorbed water) is measured as 3.24 ± 0.04 g. Accordingly, the conversion comes out to be: $\left[\left(\frac{3.24}{12.27}\right) \times 100 \right] \%$, i.e., 26.41%. On the other hand, according to the proposed reaction given by Eq 1, a total mass of 183.73 g solid reactants (123.668 g (i.e., 2 mol) of H$_3$BO$_3$ and 60.062 g (i.e., 1 mol) of CO(NH$_2$)$_2$) finally yields 49.64 g solid product (2 mol of BN). This gives a conversion of $\left[\left(\frac{49.64}{183.73}\right) \times 100 \right] \%$; i.e., 27.02%, which closely matches the actual conversion (26.41%) with only 2% deviation.

Table 2 Comparison of specific hardness of different polycrystalline materials (Ref 1-6, 8, 9, 41)

Material	Hardness, GPa	Density, g cm^{-3}	Specific hardness, GPa/g cm^{-3}
Hexagonal Al$_2$O$_3$	18-23	3.97	4.53-5.79
Cubic SiC	28-44	3.21	8.72-13.71
Hexagonal SiC	20-30	3.21	6.23-9.35
Cubic BN	33-45	3.45	9.57-13.04
Hexagonal BN	0.08	2.275	0.035
Wurtzite BN	46	3.49	13.18
Tetragonal BN (synthesized in the present investigation)	28	1.83	15.30

3.7 Band Gap and Electrical Conductivity

The experimentally determined properties of synthesized BN are summarized in Table 1. The determination of optical band gap with respect to well-known Tauc equation is shown in Fig. 4(b). Here 'h,' 'hv' and 'α' represent Planck's constant, photon energy and absorption coefficient, respectively. The experimentally determined band gap of tetragonal BN is quite large (5.66 eV). This is in agreement to a large band gap (5.38 eV) theoretically predicted by Niu and Wang (Ref 12) through Ab initio calculations for BN possessing body-centered tetragonal unit cell. Furthermore, the electrical conductivity experimentally determined with sintered BN specimen (Fig. 4c) is found to be 671 ± 18 S m^{-1} (Table 1). The electrical conductivity lies in a range of semiconductors (10^{-6}-10^4 S m^{-1}) (Ref 39). This also authenticates the semiconducting nature of tetragonal BN as per theoretical prediction by Wen et al. (Ref 10). The large band gap coupled with semiconducting behavior exemplifies potential electronic/optoelectronic applications for synthesized tetragonal BN.

3.8 Density in Correlation to Body-Centered Tetragonal Unit Cell

Furthermore, the experimentally measured density values of tetragonal BN in as-synthesized condition and in sintered condition are shown in Table 1. The density of synthesized particles (obtained in powder form) measured with normal water displacement method (using graduated measuring cylinder containing water and analytical balance) and that with Gas Pycnometer are 1.83 ± 0.02 g cm^{-3} and 1.82 ± 0.02 g cm^{-3}, respectively. Furthermore, the density of sintered pellet as measured with direct approach of weighing the pellet of known dimension and that with high precision density measurement kit are 1.75 ± 0.02 g cm^{-3} and 1.76 ± 0.01 g cm^{-3}, respectively. Such a significantly low value of density can be explained through basic theoretical calculations for a body-centered tetragonal unit cell of BN in view of atomic mass values, lattice parameters and effective number of atoms. Considering a body-centered tetragonal unit cell of one atom per lattice point and maintaining stoichiometry of BN, the effective number of atoms per unit cell for each of B and N would be 2. Now, as per the standard literature (Ref 38) atomic mass values of B and N in a.m.u. are 10.81 and 14.01, respectively. Therefore, introducing Avogadro number (6.023×10^{23} mol^{-1}), the mass of a unit cell becomes $\left[\frac{(10.81 \times 2 + 14.01 \times 2)}{6.023 \times 10^{23}}\right]$ g, i.e., 8.24×10^{-23} g. Again, obtaining lattice parameters (a = 4.38 Å, c = 2.54 Å) of body-centered tetragonal BN unit cell from the standard literature (Ref 16), the volume (a^2c) of unit cell is calculated

as: $[(4.38 \times 10^{-8})^2 \times (2.54 \times 10^{-8})]$ cm^3, i.e., 4.87×10^{-23} cm^3. Therefore, the theoretical density of tetragonal BN comes out to be $\left(\frac{8.24}{4.87}\right)$ g cm^{-3}, i.e., 1.69 g cm^{-3}. The experimentally determined density value closely matches to this theoretically calculated value. It is further interesting to note that so far in the absence of any synthesis of tetragonal BN in real practice, theoretically predicted density, as initially conceived in diffraction data file (Ref 16), is twice (3.38 g cm^{-3}) the value obtained in the present investigation due to consideration of body-centered tetragonal unit cell of BN with two atoms per lattice point. In a recent theoretical ab initio calculation, considering a BN crystal of body-centered tetragonal unit cell comprising of fourfold helical chains with complementary chirality, a much lower density value (2.43 g cm^{-3}) has been reported (Ref 12). Therefore, it appears that a crystalline BN phase of body-centered tetragonal unit cell with single atom per lattice point, possessing the lowest density reported so far, is stabilized through preferred growth of (110) planes during low-cost chemical synthesis route adopted in the present investigation. It is noteworthy to mention that the atomicity (number of atoms per lattice point) is likely to influence only the peak intensity and should not affect the position (2θ) of peaks or the lattice parameters (a,c). In accordance, the use of existing diffraction data file of tetragonal BN (Ref 16) to identify crystal structure is quite justified.

To proceed further on this conceptualization, the schematic representation of the unit cell of our proposed body-centered tetragonal BN crystal is given in Fig. 4(d) in correlation with experimentally observed atomic arrangement on (110) plane (Fig. 3d-inset). Nitrogen atoms, being larger in size for higher atomic number, form the basic body-centered tetragonal cell. On the other hand, $\frac{2}{3}$ of the octahedral void positions (face center positions) are occupied by smaller-sized boron atoms. In accordance, effective number of atoms in a unit cell for each of nitrogen and boron becomes 2 along with a single atom residing in each lattice site. The close packed (110) plane is also indicated in Fig. 4(d), preferred growth of which lowers down the system energy, thereby stabilizing the body-centered tetragonal structure of BN. This is exemplified with single dominating (110) diffraction peak in XRD analysis (Fig. 2a). Apart from correlation with existing diffraction data file of body-centered tetragonal BN (Ref 16), further authenticity in phase identification can be ascertained with basic structure factor calculation with regard to our proposed crystal structure (Fig. 4d). Now, atomic positions of nitrogen are 000 and $\frac{1}{2}\frac{1}{2}\frac{1}{2}$. In view of partial occupancy of octahedral void sites, the positions of boron atoms are given as $\frac{1}{2}\frac{1}{2}0$ and $\frac{1}{2}0\frac{1}{2}$. Therefore, considering atomic scattering factor for nitrogen and boron as

f_N and f_B, respectively, the expression of structure factor (F) comes out to be:

$$F = f_N e^{2\pi i(0)} + f_N e^{2\pi i\left(\frac{h}{2}+\frac{k}{2}+\frac{l}{2}\right)} + f_B e^{2\pi i\left(\frac{h}{2}+\frac{k}{2}\right)} + f_B e^{2\pi i\left(\frac{h}{2}+\frac{l}{2}\right)}$$

$$F = f_N + f_N e^{\pi i(h+k+l)} + f_B e^{\pi i(h+k)} + f_B e^{\pi i(h+l)}$$

$$F = f_N[1 + e^{\pi i(h+k+l)}] + f_B[e^{\pi i(h+k)} + e^{\pi i(h+l)}]$$

In case of (110) plane,

$$F = f_N(1 + e^{2\pi i}) + f_B(e^{2\pi i} + e^{\pi i}) = f_N(1 + 1) + f_B(1 - 1)$$

$$F = 2f_N; \quad F^2 = 4f_N^2$$

Therefore, the resultant intensity of scattered beam (which is proportional to F^2) from (110) plane is expected to be quite significant resulting in diffraction. This is well supported by the result of XRD analysis (Fig. 2a). Besides, preferred growth of (110) plane acts as an additional factor to enhance intensity of (110) peak to an extremely high level eclipsing other diffraction peaks. In accordance, being also authenticated by nonzero 'F' value (as per the expression of 'F' given above), (011) peak appears to be the next diffraction peak. However, its intensity is quite low due to dominance of diffraction from (110) plane that is grown preferably to lower down system energy. Again, in view of these two identifiable peaks of XRD analysis, lattice parameters (a, c) may be cross-verified. With regard to Bragg law ($\lambda = 2d\mathrm{Sin}\theta$) and the expression of interplanar spacing for tetragonal crystal system $\left(\frac{1}{d_{hkl}^2} = \frac{h^2+k^2}{a^2} + \frac{l^2}{c^2}\right)$, the relevant useful relationship is obtained as: $\frac{h^2+k^2}{a^2} + \frac{l^2}{c^2} = \frac{4\mathrm{Sin}^2\theta}{\lambda^2}$. Using this relationship, for an incident x-ray wavelength (λ) of 0.15406 nm, in view of the conditions for (110) diffraction ($\theta = 14.125°$, for $2\theta = 28.25°$) and (011) diffraction ($\theta = 20.435°$, for $2\theta = 40.87°$) as obtained experimentally (Fig. 2a), the lattice parameters are calculated as: $a = 0.4464$ nm and $c = 0.2538$ nm. These values are quite close to those measured experimentally from electron diffraction analysis ($a = 0.4378$ nm, $c = 0.2541$ nm) and those predicted theoretically ($a = 0.4380$ nm, $c = 0.2540$ nm) for body-centered tetragonal BN in the standard literature (Ref 16).

3.9 Specific Hardness

The detailed result of hardness measurement is shown in Fig. 4(e). Furthermore, the close similarity between the x-ray diffractogram of the sintered BN specimen (Fig. 4f) and that of the as-synthesized BN particles (Fig. 2a) confirms no major phase change on sintering. This also authenticates the hardness measurement of tetragonal BN. The measured hardness value (28 ± 1 GPa) of tetragonal BN is quite high (Table 1). This is in accordance with strong SP^3 B-N bond formation evolving three-dimensional tetragonal crystal network as theoretically predicted by Li and Gao (Ref 11) and exemplified as well in the present work with Raman spectroscopy and x-ray photoelectron spectroscopy results (Fig. 2c, d, e, and f). In addition, a wide-band gap (5.66 eV) indicates a large concentration of valence electrons, which, in turn, is expected to enhance hardness of BN crystal (Ref 40). Furthermore, in polycrystalline form, the measured mean crystal size of synthesized tetragonal BN is also small and in submicroscopic range (163 nm). This, as per well-known Hall–Petch effect, is expected to provide high hardness

(Ref 1). Most interestingly, as shown in Table 2, by virtue of an adequate combination of high hardness and low density, the synthesized tetragonal BN possesses the highest specific hardness (hardness per unit density) value of 15.30 GPa/ g cm^{-3}, when compared with different polymorphs of BN or other common hard ceramic materials in polycrystalline form (Ref 1-6, 8, 9, 41). With regard to recent research works on structural composite materials (Ref 42), the specific hardness property for reinforcement particle is believed to be an important property (Ref 43) to decide specific strength property of composite materials in view of load transfer from matrix to reinforcement particle. Therefore, the high specific hardness property attributes to the potential of synthesized BN particles for being used as reinforcement in metal matrix composites for energy-saving high-strength low-density structural application.

4. Conclusion

1. The synthesis of tetragonal BN, a novel polymorph of BN, is made practically feasible through a low-cost chemical route for the first time so as to add a new dimension in material development.
2. The chemical reaction feasibility to originate BN is verified on thermodynamic perspective as well as through experimentation for ascertaining the evolution of product phases.
3. The body-centered tetragonal structure of a three-dimensional network is experimentally ascertained for the synthesized BN in terms of peak position by XRD analysis, interplanar spacing along with lattice parameter determination by FEG-TEM analysis and sp^3-bonding characteristics by Raman spectroscopy and XPS analysis.
4. The experimentally obtained properties are quite interesting; that includes wide-band gap, low electrical conductivity in the semiconducting range and significantly high specific hardness.
5. This envisages an authentic scope for futuristic applications of this novel material in electronic/optoelectronic field and usages in the development of energy-saving structural materials.

Conflict of interest

The authors declare that they have no conflict of interest.

References

1. Y. Tian, B. Xu, D. Yu, Y. Ma, Y. Wang, Y. Jiang, W. Hu, C. Tang, Y. Gao, K. Luo, Z. Zhao, L.-M. Wang, B. Wen, J. He, and Z. Liu, Ultra Hard Nanotwinned Cubic Boron Nitride, *Nature*, 2013, **493**, p 385–388
2. R.H. Wentorf, R.C. DeVries, and F.P. Bundy, Sintered Superhard Materials, *Science*, 1980, **208**, p 873–880

3. W.Y.H. Liew, S. Yuan, and B.K.A. Ngoi, Evaluation of Machining Performance of STAVAX with PCBN Tools, *Int. J. Adv. Manuf. Technol.*, 2004, **23**, p 11–19

4. C.B. Samantaray and R.N. Singh, Review of Synthesis and Properties of Cubic Boron Nitride (c-BN) Thin Films, *Int. Mater. Rev.*, 2005, **50**, p 313–344

5. Y. Liu, G.D. Zhan, Q. Wang, D. He, J. Zhang, A. Liang, T.E. Moellendick, L. Zhao, and X. LI, Hardness of Polycrystalline Wurtzite boron Nitride (wBN) Compacts, *Sci. Rep.*, 2019, **9**, p 1–6. https://doi.org/10.1038/s41598-019-46709-4

6. T.B. Wang, C.C. Jin, J. Yang, C.F. Hu, and T. Qiu, Physical and Mechanical Properties of Hexagonal Boron Nitride Ceramic Fabricated by Pressureless Sintering Without Additive, *Adv. Appl. Ceram.*, 2015, **114**, p 273–276

7. D.A. Evans, A.G. McGlynn, B.M. Towlson, M. Gunn, D. Jones, T.E. Jenkins, R. Winter, and N.R.J. Poolton, Determination of the Optical Band-Gap Energy of Cubic and Hexagonal Boron Nitride Using Luminescence Excitation Spectroscopy, *J. Phys.: Condens. Matter.*, 2008, **20**, p 1–7

8. C. Steinborn, M. Herrmann, U. Keitel, A. Schönecker, J. Rathel, D. Rafaja, and J. Eichler, Correlation Between Microstructure and Electrical Resistivity of Hexagonal Boron Nitride Ceramics, *J. Eur. Ceram. Soc.*, 2013, **33**, p 1225–1235

9. Anon, Ioffe Institute Database, St Petersburg 194021, Russian Federation, 2019. www.ioffe.ru/SVA/NSM/Semicond/BN/index.html

10. B. Wen, J. Zhao, R. Melnik, and Y. Tian, Body-Centered Tetragonal B2N2: A Novel sp^3 Bonding Boron Nitride Polymorph, *Phys. Chem. Chem. Phys.*, 2011, **13**, p 14565–14570

11. Z. Li and F. Gao, Structure, Bonding, Vibration and Ideal Strength of Primitive-Centered Tetragonal Boron Nitride, *Phys. Chem. Chem. Phys.*, 2012, **14**, p 869–876

12. C.-Y. Niu and J.-T. Wang, Three-Dimensional Three-Connected Tetragonal BN: Ab Initio Calculations, *Phys. Lett. A*, 2014, **378**, p 2303–2307

13. S. Zhang, Q. Wang, Y. Kawazoe, and P. Jena, Three-Dimensional Metallic Boron Nitride, *J. Am. Chem. Soc.*, 2013, **135**, p 18216–18221

14. K. Gao, Y. Xu, W. Song, L. Guan, M. Li, K. Li, X. Guo, and R. Zhang, Preparation and Growth Characterization of Al₂Cu Phase Crystal with the Single Orientation Under Directional Solidification, *Mater. Res.*, 2018, **21**, e20180381. https://doi.org/10.1590/1980-5373-MR-2018-0381

15. D.B. Gadkari, P. Shashidharan, K.B. Lal, and B.M. Arora, Influence of Crystal-Melt Interface Shape on Self-seeding and Single Crystalline Quality, *Bull. Mater. Sci.*, 2001, **24**, p 475–482

16. K. Doll, J.C. Schoen and M. Jansen, Structure Prediction Based on Ab Initio Simulated Annealing for Boron Nitride, Phys. Rev. B, **78**, 1–10, 2008. (Article number: 144110). (Cross Reference: *JCPDS*-International Centre for Diffraction Data, Reference code: 98-011-5787, File No. 98-000-0274)

17. R.S. Pease, An x-ray Study of Boron Nitride, Acta Cryst., **5**, 356–361, 1952. (Cross Reference: *JCPDS*-International Centre for Diffraction Data, Reference code: 98-000-8575, File No. 98-000-0274)

18. L. Li, Y. Bi, C. Ban, H. Zhang, T. Liu, X. Wang, C. Esling, and J. Cui, A Crystallographic Study on the Growth of Partially Faceted MnSn₂ Phase during Solidification Process, *Crystals*, 2018, **380**, p 1–6. https://doi.org/10.3390/cryst8100380

19. P. Soundarrajan, K. Sankarasubramanjan, K. Sethuraman, and K. Ramamurthi, Controlled (110) and (101) Crystallographic Plane Growth of Single Crystalline Rutile TiO₂ Nanorods by Facile Low Cost Chemical Methods, *Cryst. Eng. Commun.*, 2014, **16**, p 8756–8768. https://doi.org/10.1039/c4ce00820k

20. O. Lupan, L. Chow, G. Chai, H. Heinrich, S. Park, and A. Schulte, Growth of Tetragonal SnO₂ Microcubes and Their Characterization, *J. Crystal Growth*, 2008, **311**, p 152–155

21. A.R. Dhamdhere, T. Hadamek, A.B. Posadas, A.A. Demkov, and D.J. Smith, Structural Characterization of Niobium Oxide Thin Films Grown on SrTiO₃ and (La, Sr) (Al, Ta) O₃ (111) Substrates, *J. Appl. Phys.*, 2016, **120**, p 1–6

22. R.A. Dunlap, The Symmetry and Packing Fraction of the Body Centered Tetragonal Structure, *Eur. J. Phys. Educ.*, 2012, **3**, p 19–24

23. T.H.K. Barron and C. Domb, On the Cubic and Hexagonal Close-Packed Lattices, *Proc. R. Soc. (Lond.) Ser. A*, 1955, **227**, p 447–465

24. W.D.S. Motherwell, Architecture of Packing in Molecular Crystals, *Cryst. Eng. Commun.*, 2017, **19**, p 6869–6882

25. A.M. Reilly, R.I. Cooper, C.S. Adjiman, S. Bhattacharya, A.D. Boese, J.G. Brandenburg et al., Report on the Sixth Blind Test Of Organic Crystal Structure Prediction Methods, *Acta Crystallogr. B: Struct. Sci.*, 2016, **72**, p 439–459

26. S. Reich, A.C. Ferrari, R. Arenal, A. Loiseau, I. Bello, and J. Robertson, Resonant Raman Scattering in Cubic and Hexagonal Boron Nitride, *Phys. Rev. B*, 2005, **71**, p 205201

27. J.A. Sanjurjo, E. Lopez-Cruz, P. Vogl, and M. Cardona, Dependence on Volume of the Phonon Frequencies and Their Effective Charges of Several III-V Semiconductors, *Phys. Rev. B*, 1983, **28**, p 4579–4584

28. M.I. Eremets, M. Gauthier, A. Polian, J.C. Chervin, J.M. Besson, G.A. Dubitskii, and Y.Y. Semenova, Optical Properties Of Cubic Boron Nitride, *Phys. Rev. B*, 1995, **52**, p 8854–8863

29. L. Bergman and R.J. Nemanich, Raman Spectroscopy for Character-ization of Hard, Wide-Bandgap Semiconductors: Diamond, GaN, GaAlN, AlN, BN, *Ann. Rev. Mater. Sci.*, 1996, **26**, p 551–579

30. R. Geick, C.H. Perry, and G. Rupprecht, Normal Modes in Hexagonal Boron Nitride, *Phys. Rev.*, 1966, **146**, p 543–547

31. R.J. Nemanich, S.A. Solin, and R.M. Martin, Light Scattering Study of Boron Nitride Microcrystals, *Phys. Rev. B*, 1981, **23**, p 6348–6356

32. S. Joseph, "Characterization of Cubic Boron Nitride Interfaces with in situ Photoelectron Spectroscopy", Ph.D. Thesis, Arizona State University, 2016

33. M. Filippi and L. Callari, Measuring the Energy of the Graphite π + σ Plasmon Peak, *Surf. Interface Anal.*, 2006, **38**, p 595–598

34. M. Terauchi, Electronic Structure Analyses of BN Network Materials Using High Energy Resolution Spectroscopy Methods Based on Transmission Electron Microscopy, *Microscopy Res. Tech.*, 2006, **68**, p 531–537

35. P. Widmayer, H.-G. Boyen, and P. Ziemann, Electron Spectroscopy on Boron Nitride Thin Films: Comparison of Near-Surface to Bulk Electronic Properties, *Phys. Rev. B*, 1999, **59**, p 5233–5241

36. D.H.A. Besisa, M.A.A. Hagras, E.M.M. Ewais, Y.M.Z. Ahmed, Z.I. Zaki, and A. Ahmed, Low Temperature Synthesis of Nano-crystalline h-Boron Nitride from Boric Acid/Urea Precursors, *J. Ceram. Proc. Res.*, 2016, **17**, p 1219–1225

37. L. Duan, Z. Changrui, L. Bin, C. Feng, W. Siqing, L. Kun, and F. Zhenyu, Low-cost Preparation of Boron Nitride Ceramic Powders, *J. Wuhan Univ. Technol.*, 2012, **27**, p 534–537

38. J.F. Shackelford, *Introduction to Materials Science for Engineers*, Macmillan Publishing Co, New York, 1992, p 738

39. W.D. Callister, Jr., *Materials Science and Engineering*, Wiley, New Delhi, 2007, p 626

40. Z. Zhao, B. Xu, and Y. Tian, Recent Advances in Superhard Materials, *Ann. Rev. Mater. Res.*, 2016, **46**, p 4.1–4.24

41. Anon, "Ceramics and Glasses", Engineering Materials Handbook, Vol.4, ASM International, The Materials Information Society, Ohio, 1991, p 30

42. U.G.K. Wegst, H. Bai, E. Saiz, A.P. Tomsia, and R.O. Ritchie, Bioinspired Structural Materials, *Nat. Mater.*, 2015, **14**, p 23–36

43. A. Banerjee, V. Tungala, K. Sala, K. Biswas, and J. Maity, A Comparative Study on the Dry Sliding Wear Behaviour of Mild Steel and 6061Al-15 wt.% SiCₚ Composite, *J. Mater. Eng. Perform.*, 2015, **24**, p 2303–2311. https://doi.org/10.1007/s11665-015-1508-z